

Anisotropic Spectral-Spatial Total Variation Model for Multispectral Remote Sensing Image Destriping

Yi Chang, Luxin Yan, *Member, IEEE*, Houzhang Fang, *Student Member, IEEE*, and Chunan Luo

Abstract—Multispectral remote sensing images often suffer from the common problem of stripe noise, which greatly degrades the imaging quality and limits the precision of the subsequent processing. The conventional destriping approaches usually remove stripe noise band by band, and show their limitations on different types of stripe noise. In this paper, we tentatively categorize the stripes in remote sensing images in a more comprehensive manner. We propose to treat the multispectral images as a spectral-spatial volume and pose an anisotropic spectral-spatial total variation regularization to enhance the smoothness of solution along both the spectral and spatial dimension. As a result, a more comprehensive stripes and random noise are perfectly removed, while the edges and detail information are well preserved. In addition, the split Bregman iteration method is employed to solve the resulting minimization problem, which highly reduces the computational load. We extensively validate our method under various stripe categories and show comparison with other approaches with respect to result quality, running time, and quantitative assessments.

Index Terms—Destriping, denoising, spectral-spatial total variation, split Bregman iteration, remote sensing image.

I. INTRODUCTION

REMOTE sensing images normally consist of dozens or even hundreds of spectral bands, and have been drawn many attentions from various application fields, such as detecting minerals, urban planning, precision farming, etc. Unfortunately, the stripe noise in multispectral images not only greatly influences the visual quality of these images but also limits the precision of the further processing, for instance, in

Manuscript received July 21, 2014; revised December 28, 2014; accepted February 3, 2015. Date of publication February 18, 2015; date of current version March 27, 2015. This work was supported in part by the Fundamental Research Funds for the Central Universities, Huazhong University of Science and Technology, Wuhan, China, under Grant 2013TS131 and in part by the National Natural Science Foundation of China under Grant 61433007 and Grant 60902060. The associate editor coordinating the review of this manuscript and approving it for publication was Dr. Sylvain Paris.

Y. Chang, L. Yan, and C. Luo are with the Science and Technology on Multispectral Information Processing Laboratory, School of Automation, Huazhong University of Science and Technology, Wuhan 430074, China (e-mail: owuchangyu@gmail.com; yanluxin@gmail.com; chunanluo@gmail.com).

H. Fang is with the National Laboratory of Radar Signal Processing, Xidian University, Xi'an 710071, China (e-mail: houzhangfang@gmail.com).

This paper has supplementary downloadable material available at <http://ieeexplore.ieee.org>, provided by the author. The material includes additional information and figures that are not included in the paper itself. The total size of the file is 133 kB. Contact yanluxin@gmail.com for further questions about this work.

Color versions of one or more of the figures in this paper are available online at <http://ieeexplore.ieee.org>.

Digital Object Identifier 10.1109/TIP.2015.2404782

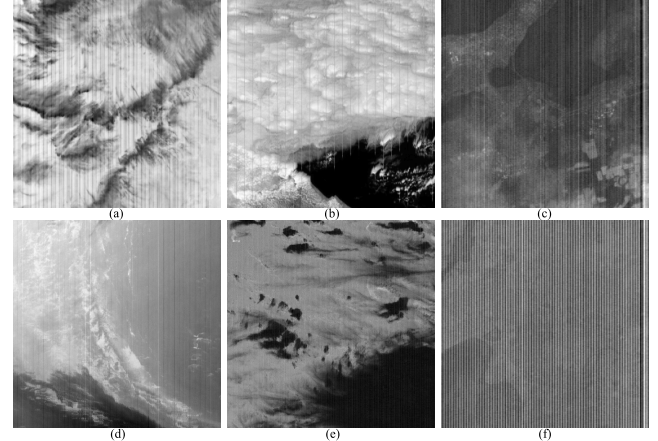


Fig. 1. Categorization of stripes. (a) Regular periodic stripes. (b) Periodic stripes with discontinuity. (c) Non-periodic stripes with random width. (d) Non-periodic stripes with random length. (e) Mild stripes with mild random noise. (f) Severe stripes with severe random noise.

classification, unmixing, target detection, etc. [1]–[4]. Therefore, it is critical to suppress the stripes in the multispectral image and improve its quality before the succeeding image interpretation processes. The goal of this work is to remove the stripe and improve its quality before the subsequent interpretation.

A. Categorization of Stripes

In multispectral remote sensing imaging systems of two different types, push-broom and cross-track imaging devices, the stripes are mainly caused by relative gain and/or offset differences in response of the detectors. The striping effect has different characteristics, depending on the scanning mechanism of imaging instruments. In previous works, most of the destriping methods are designed for specific satellite imaging instruments, for instance for cross-track type [5] and push-broom type [6]. These specific destriping methods suggest different tactics according to the type of the stripes, thus are lack of robustness to a variety of stripes. To the best of our knowledge, few works on comprehensive striping categorization for both cross-track and push-broom sensors have been attempted. In this work, according to the characteristic of stripes in images, we firstly classify the stripe images into six categories illustrated in Fig. 1.

The most common and easy to be removed stripe noise is the regular periodic stripe. The periodic stripes corresponding to the number of detectors always appear in the cross-track scanning sensors, such as Moderate Resolution Imaging

Spectroradiometer (MODIS) and Landsat Thematic Mapper (TM). For example, in Fig. 1(a), there exist eight stripe lines per ten lines, including six successive stripe lines with different variances. These periodic stripes can be observed over a whole swath and are usually caused from the slight deviations between adjacent detectors. The stripes, in Fig. 1(b), are also periodic but exhibit discontinuity in single stripe line per ten lines. Due to the non-integrity characteristic within a scan line, these stripes are hardly removed by conventional methods.

The third case is the stripes being non-periodic, as shown in Fig. 1(c), which usually occur in push-broom imaging spectrometer, such as Hyperion onboard Earth Observation-1 (EO-1) and Satellite Pour l'Observation de la Terre (SPOT). These stripes arise from the unstable detectors during a scanning cycle. They appear as bright or dark lines with random widths. Even worse, some dead pixels are distributed in the image, which do not convey any useful information. In Fig. 1(d), the stripes are also non-periodic, while they appear as bright and dark lines with random lengths within a scan line, caused from the residual calibration errors of the internal calibration system. These stripes as shown in Fig. 1(d) usually appear in cross-track scanning sensors systems.

In the fifth case, stripes and random noise coexist in the images [5]–[9], for example in Fig. 1(e). Conventional methods usually treat the stripe noise and random noise issue separately. However, it is time-consuming and may suffer from defective output for the mutual interference with each other [10]. Therefore, we tend to regard this case as a new stripe category and remove both the stripes and random noise simultaneously. In Fig. 1(f), the image information is almost overwhelmed by severe stripes and random noise, which makes it impossible to recover useful information from single band image.

B. Related Destriping Algorithms

In recent decades, many remote sensing image destriping algorithms have been proposed. Corresponding to different stripes, there are three main kinds of approaches for removing specific stripes in remote sensing image. The first kind of destriping approaches is the digital filtering technique, such as low-pass filter [11], wavelet analysis [12], and the Fourier-wavelet combined domain filter [13]. These methods mainly focus on suppressing the specific frequencies caused by stripes in transformed domain, and follow the assumption that stripes are periodic and can be identified from the power spectrum. These digital filtering methods are easy to be implemented but only work well for the periodic stripes in cross-track scanning sensors. However, the details with the same frequencies will also be affected along with the stripes, thereby leading to image blurring and artifacts. For example, Munch *et al.* [13] proposed a Fourier and wavelet combined filter with fast and impressive destriping results, which fully excavated the directional characteristic of the stripes via wavelet decomposition. Some destriping methods [6], [14] first detected the stripe lines and then made use of the interpolation

strategy to remove the stripes. Their performances heavily depend on the accuracy of stripes detection.

Another class of destriping approaches focuses on the statistical property of digital numbers (DNs) for each detector. To remove the stripes, the distribution of stripes is rectified to a reference distribution, such as moment matching [15] and histogram matching [16]. The former assumes that the mean and standard deviation of each detector are identical, while the latter assumes the distributions of each detector in a large scene are similar. These matching-based methods can get satisfactory destriping results when the scenes are simple and homogeneous. However, their performances are highly limited because the strong similarity assumptions [17] are always invalid. Wegner [17] proposed a method to overcome this limitation by calculating the statistics only over homogeneous image regions. Furthermore, some hybrid approaches combining statistical methods with advanced image processing techniques have been suggested. In [5], the authors combined histogram matching with facet filter to reduce stripe noise in MODIS data. To some extent, the facet filter could suppress the residual noise and random noise. Radiometric equalization-based approach was also applied to remove non-periodic stripes [18].

Recently, some interesting works regarded the destriping issue as an ill-posed inverse problem [19]–[27], and then optimized variational model incorporating some priors about the image to obtain the desired destriping results. In 2009, Shen and Zhang [19] firstly proposed a maximum-a-posteriori destriping and inpainting method with a Huber-Markov prior, which can be viewed as an alternative between total variation (TV) regularization and Tikhonov regularization. In [21], the authors proposed a more sophisticated unidirectional TV model and made use of the directional information of the stripes. However, because of the excessive constraints on the unidirectional derivative, structural details with the same direction as stripes are inevitably removed along with the stripes. In our recent work [23], we presented a joint unidirectional TV and framelet regularization method to remove stripes as well as preserve structural details. Fehrenbach *et al.* [25] proposed a simple class of parametric random processes that describes the stripes named variational stationary noise remover (VSNR). Instead of estimating the clear image, they made use of the Huber-Markov prior to estimate the stripe components. Taking the random noise into consideration, we recently have proposed a simultaneous destriping and denoising method by combining unidirectional total variation and sparse representation [10].

C. Proposed Algorithm

The multispectral or hyperspectral image cube usually consists of two spatial dimensions (along track and across track) and one spectral dimension (wavelength), as illustrated in Fig. 2. The spectral dimension provides extra complementary information. Taking use of the information both in spatial and spectral domains can help improve restoration performance. It is worth noting that most of the aforementioned destriping methods remove the striping effects in

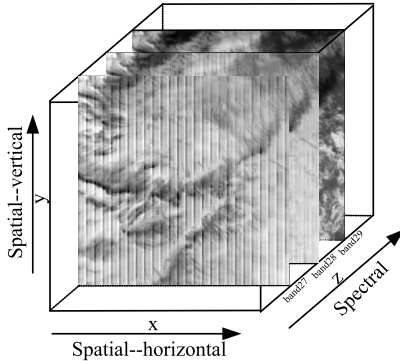


Fig. 2. Illustration of the remote sensing spectral-spatial cube.

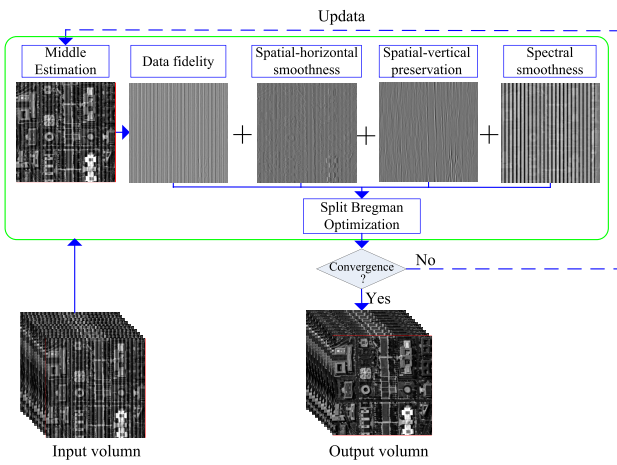


Fig. 3. The framework of the proposed ASSTV model.

a single band. The drawback of processing each band of image in band-by-band manner is that it will lose the consistency between consecutive bands. In fact, there are many remote sensing denoising methods utilizing the spectral information to improve their performances, such as spectral-spatial adaptive total variation [9], 3D wavelets [34], and nonlocal spectral-spatial structured sparse representation [35]. Therefore, how to utilize the spectral information in multispectral image destriping is a noteworthy point. Only recently, two hyperspectral image destriping approaches using low rank matrix to exploit the high spectral correlation have also been proposed [26], [27]. In this paper, from a spectral-spatial smoothness perspective, we propose an anisotropic spectral-spatial total variation (ASSTV) model for multispectral image destriping, in which the stripes differences between different bands and spatial property differences in spatial domain are both considered.

While ASSTV belongs to the variation-based destriping scheme, it is implemented through a novel prior that combines anisotropic spatial smoothness and spectral smoothness. The former utilizes the spatial directional characteristic of the stripes to remove the stripes and preserve the edge information, while the latter enforces the spectral consistency constraint to help remove the severe stripes and random noise, so as to obtain the robustness to various stripes. The main ideas and

contributions of the proposed approach can be summarized as follows.

- 1) The proposed method treats the multispectral or hyperspectral remote sensing images as a spectral-spatial cube and considers the consistency of the remote sensing images in both the spectral and spatial domains, so as to better remove the stripes.
- 2) A comprehensive categorization of the stripes is proposed. We have shown the proposed method is robust in different striping cases, even resilient in extreme large amounts of noise.
- 3) To make the algorithm simple and fast to implement, we extend the split Bregman method to solve the spectral-spatial 3D TV minimization problem, in which the optimization of the destriping model is split into several easier subproblems.

D. Organization of This Paper

The remainder of this paper is organized as follows. The proposed ASSTV destriping model is described in Section II. In Section III, the optimization process by split Bregman method is presented in detail. Section IV presents the experimental results and discusses various aspects of the proposed method. Finally, Section V concludes this paper.

II. ANISOTROPIC SPECTRAL-SPATIAL TOTAL VARIATION DESTRIPIING MODEL

A. Problem Formulation

In multispectral or hyperspectral remote sensing image cube, the striping effect is assumed to be additive noise, and the stripes degradation model can be written as

$$f(m, n, k) = u(m, n, k) + n(m, n, k), \quad (1)$$

where $m = 1, 2, \dots, M$, $n = 1, 2, \dots, N$, and $k = 1, 2, \dots, K$. M and N stand for the number of the rows and columns in each band respectively, and K is the number of sensor bands. Here, $f(m, n, k)$, $u(m, n, k)$, and $n(m, n, k)$ represent the degraded image, the ground-truth image, and the noise of the location (m, n) in the k -th band, respectively. Note that, the noise n in this work includes both stripe noise and random noise.

For the purpose of discussing numerical algorithm, we write the model (1) in matrix-vector form

$$\mathbf{f} = \mathbf{u} + \mathbf{n}, \quad (2)$$

where \mathbf{f} , \mathbf{u} , and \mathbf{n} represent the vectorized version of f , u and n , respectively, by stacking each of them into a long column vector of size $MNK \times 1$ according to the lexicographical order. For instance, $\mathbf{f} = [\text{vec}(f_1); \text{vec}(f_2); \dots; \text{vec}(f_K)] \in \mathbf{R}^{MNK \times 1}$, in which $\text{vec}(f_k)$ ($k = 1, 2, \dots, K$) denotes the vectorized observation image in the k -th band.

In this work, the destriping task is formulated as an ill-posed inverse problem. Formally, our destriping task is to estimate the latent clear image cube \mathbf{u} from the given image cube \mathbf{f} in the presence of both stripes and random noise \mathbf{n} . Based on the regularization theory, the destriping model can be formulated

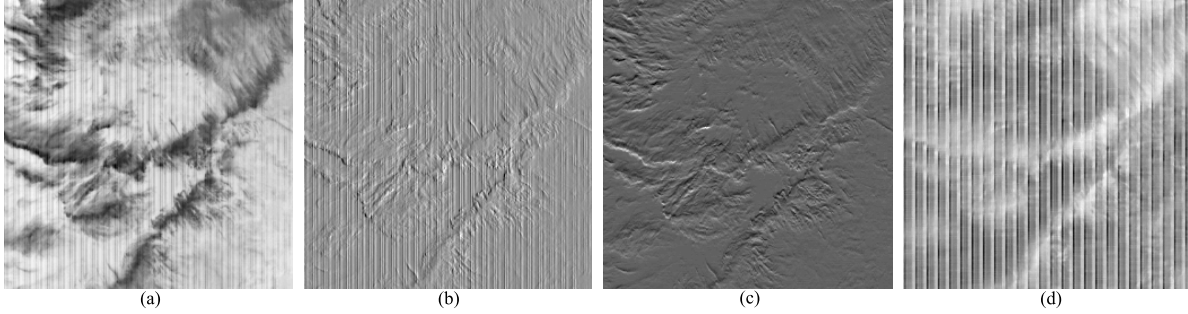


Fig. 4. Directional characteristic of stripes in remote sensing cube. (a) Original MODIS image band 27. (b) Spatial horizontal gradient. (c) Spatial vertical gradient. (d) Spectral gradient.

as the combination of the data fidelity term and regularization term as follows:

$$\hat{\mathbf{u}} = \arg \min_{\mathbf{u}} \frac{1}{2} \|\mathbf{u} - \mathbf{f}\|_2^2 + \lambda R(\mathbf{u}) \quad (3)$$

The first term in (3) is the data fidelity term, which provides the similarity between the desired clear image and degraded image. The second term is the regularization term by imposing constraints on the image, aiming at penalizing the undesirable properties in images. λ is the regularization parameter, which controls the tradeoff between the data fidelity and regularization terms. The key is to construct appropriate regularization terms to constrain the solution so as to remove the stripes.

B. TV Model

In past decades, TV-based regularizations have been widely used in various applications [28]–[30], due to their desirable properties such as convexity and the ability to preserve sharp edges. Rudin *et al.* [29] first introduced the TV model as follows:

$$\|\mathbf{u}\|_{\text{TV}} = \sum_i \sqrt{(\mathbf{D}_x \mathbf{u})_i^2 + (\mathbf{D}_y \mathbf{u})_i^2} \quad (4)$$

where \mathbf{D}_x and \mathbf{D}_y are linear operators corresponding to the horizontal and vertical first-order differences, respectively, at pixel i . A straightforward way of extending the TV model in (4) to multispectral images is to add up the TV model of each band in a band-by-band fashion. Traditional methods with operating on each band independently like (4) should adjust their constraints hand by hand in different bands, which may lead to the loss of the spectral consistency. Moreover, some bands with highly contaminated noise cannot be well restored with only the spatial information. Therefore, it is worthwhile to incorporate the spectral information to the traditional TV model.

C. Spectral-Spatial TV Model

As multispectral images have dozens or even hundreds of bands, the pattern of the stripes in each band are different. To some extent, these differences in multispectral images provide extra complementary information. And the spectral domain exhibits much fewer variations in terms of patterns

than the spatial domain [31]. Therefore, we argue that stripe noise and random noise are advantageous to be removed from both the spatial and spectral domains by enforcing smooth constraints onto the image cube both along the spatial and spectral dimension, somewhat analogous to the spatial and temporal consistency strategies in video restoration [32], [33]. So, we can extend the traditional TV model in (4) to define the isotropic spectral-spatial TV model as follows:

$$\|\mathbf{u}\|_{\text{SSTV}} = \sum_i \sqrt{(\mathbf{D}_x \mathbf{u})_i^2 + (\mathbf{D}_y \mathbf{u})_i^2 + (\mathbf{D}_z \mathbf{u})_i^2} \quad (5)$$

where the operators \mathbf{D}_x , \mathbf{D}_y , and \mathbf{D}_z are the first-order forward finite-difference operators along the x-axis (horizontal direction), y-axis (vertical direction), and z-axis (spectral direction), respectively. The subscript i denotes the pixel's index in the image cube. The definitions of the finite-difference operators are

$$\begin{cases} \mathbf{D}_x \mathbf{u}(x, y, z) = u(x+1, y, z) - u(x, y, z) \\ \mathbf{D}_y \mathbf{u}(x, y, z) = u(x, y+1, z) - u(x, y, z) \\ \mathbf{D}_z \mathbf{u}(x, y, z) = u(x, y, z+1) - u(x, y, z) \end{cases} \quad (6)$$

with periodic boundary conditions. By enforcing the constraints on both spatial and spectral dimensions, the piecewise smooth property on both directions can be guaranteed.

D. Anisotropic Spectral-Spatial TV Model for Destriping

The spectral-spatial TV (SSTV) is effective for random noise removal [5]. However, unlike random noise, the stripes exhibit significantly structural characteristic. In the destriping process, the stripes are easy to be treated as the large edges by the isotropic TV model. As a result, the SSTV model tends to suppress the stripes at the cost of damaging the useful edges and detail information. Moreover, due to the clearly directional characteristic of the stripes, it is easy to introduce obvious blurring artifacts by the isotropic model [21]. To illustrate the directional characteristic of the stripes, in Fig. 4, we show the derivatives of the remote sensing volume at three directions. The original MODIS image band 27 is shown in Fig. 4(a), and the derivatives of the volume along the x-axis, y-axis, and z-axis are shown in Figs. 4(b)-4(c), respectively. The spectral gradient of one point is defined as the forward difference along the spectral direction between two neighbor bands. In clear remote sensing cube, the spectral gradient should be

rather smooth. However, due to the stripe noise, it is observed that the stripes severely damage the spatial horizontal gradient [Fig. 4(b)] and spectral gradient [Fig. 4(d)], while the spatial vertical gradient [Fig. 4(c)] is not influenced at all.

This observation motivates us to constrain the gradients on both the spatial horizontal (x-axis) and spectral directions (z-axis) while preserving the gradient as the degraded image on the spatial vertical direction (y-axis). To do this, we extend the isotropic spectral-spatial TV to the anisotropic spectral-spatial TV as follow:

$$\|\mathbf{u}\|_{\text{ASSTV}} = \sum_i (\lambda_1 |(\mathbf{D}_x \mathbf{u})_i| + \lambda_2 |(\mathbf{D}_y (\mathbf{u} - \mathbf{f}))_i| + \lambda_3 |(\mathbf{D}_z \mathbf{u})_i|) \quad (7)$$

where λ_1 , λ_2 , and λ_3 are the regularization parameters. Substituting $R(\mathbf{u})$ by ASSTV regularization in (7), we introduce the final energy functional about \mathbf{u} as:

$$\min_{\mathbf{u}} \frac{1}{2} \|\mathbf{u} - \mathbf{f}\|_2^2 + \lambda_1 \|\mathbf{D}_x \mathbf{u}\|_1 + \lambda_2 \|\mathbf{D}_y (\mathbf{u} - \mathbf{f})\|_1 + \lambda_3 \|\mathbf{D}_z \mathbf{u}\|_1. \quad (8)$$

We explain each term of the model in detail as follows:

- 1) The first term is the reconstruction constraint, i.e., the recovered result should be consistent with the observation according to the observed model.
- 2) The second term penalizes the ℓ_1 -norm of the gradient across the stripe line, so as to suppress the stripes. In other words, it favors a solution \mathbf{u} that its derivative along the x-axis is rather smooth.
- 3) The third term enforces the ℓ_1 -norm constraint on the difference between the gradients along the stripe of the desired and striped images, aiming to preserve the gradient along the stripe. It is very reasonable since the stripes have little influence on the gradient along the stripes.
- 4) The fourth term penalizes the ℓ_1 -norm of the gradient along the spectral direction, so as to preserve the spectral consistency. The stripes and random noise are random distributed in each band, leading to the large spectral discontinuity. Penalizing the ℓ_1 -norm of the spectral gradient will help suppress the stripes and random noise as well as preserving the spectral details.

The flowchart of the proposed method is illustrated in Fig. 3. In summary, the basic idea of the model is to penalize the gradients across the stripes of the desired image while preserving the gradients along the stripes of the desired image as the degraded image; meanwhile, the destriped image cube should keep the spectral consistency.

III. SPLIT BREGMAN OPTIMIZATION

The difficulties in determining \mathbf{u} from (8) are that the ℓ_1 -norm terms are nondifferentiable. The split Bregman iteration proposed by Tom Goldstein in [36] is efficient to solve the

ℓ_1 -norm-based regularization, such as the TV model. In this section, the split Bregman iteration is extended to optimize the proposed ASSTV destriping model in (8) to solve the 3D image cube \mathbf{u} . The main idea is to convert the unconstrained minimization problem on \mathbf{u} in (8) into a constrained one by introducing three auxiliary variables $\mathbf{d}_x = \mathbf{D}_x \mathbf{u}$, $\mathbf{d}_y = \mathbf{D}_y (\mathbf{u} - \mathbf{f})$, and $\mathbf{d}_z = \mathbf{D}_z \mathbf{u}$. The minimization of (8) is equivalent to the constrained problem

$$\begin{aligned} & \min_{\mathbf{u}} \frac{1}{2} \|\mathbf{u} - \mathbf{f}\|_2^2 + \lambda_1 \|\mathbf{d}_x\|_1 + \lambda_2 \|\mathbf{d}_y\|_1 + \lambda_3 \|\mathbf{d}_z\|_1 \\ & \text{s.t. } \mathbf{d}_x = \mathbf{D}_x \mathbf{u}, \mathbf{d}_y = \mathbf{D}_y (\mathbf{u} - \mathbf{f}), \mathbf{d}_z = \mathbf{D}_z \mathbf{u}. \end{aligned} \quad (9)$$

Subsequently, by strictly applying the Bregman iteration, the problem (9) can further be transformed into an unconstrained minimization

$$\begin{aligned} & \min_{\mathbf{u}, \mathbf{d}_x, \mathbf{d}_y, \mathbf{d}_z} \frac{1}{2} \|\mathbf{u} - \mathbf{f}\|_2^2 + \lambda_1 \|\mathbf{d}_x\|_1 + \lambda_2 \|\mathbf{d}_y\|_1 + \lambda_3 \|\mathbf{d}_z\|_1 \\ & + \frac{\alpha}{2} \|\mathbf{d}_x - \mathbf{D}_x \mathbf{u} - \mathbf{b}_x\|_2^2 + \frac{\beta}{2} \|\mathbf{d}_y - \mathbf{D}_y (\mathbf{u} - \mathbf{f}) - \mathbf{b}_y\|_2^2 \\ & + \frac{\gamma}{2} \|\mathbf{d}_z - \mathbf{D}_z \mathbf{u} - \mathbf{b}_z\|_2^2. \end{aligned} \quad (10)$$

where α , β , and γ denote the Bregman penalization parameters, the variable \mathbf{b}_x , \mathbf{b}_y and \mathbf{b}_z are determined via Bregman iteration. An alternative way to solve the problem in (10) is alternating minimization scheme, iteratively optimizing one variable while fixing others. Thus, the functional (10) can be converted into four simpler minimization subproblems.

- The \mathbf{u} -related subproblem is

$$\begin{aligned} & \min_{\mathbf{u}} \frac{1}{2} \|\mathbf{u} - \mathbf{f}\|_2^2 + \frac{\alpha}{2} \|\mathbf{d}_x^k - \mathbf{D}_x \mathbf{u} - \mathbf{b}_x^k\|_2^2 \\ & + \frac{\beta}{2} \|\mathbf{d}_y^k - \mathbf{D}_y (\mathbf{u} - \mathbf{f}) - \mathbf{b}_y^k\|_2^2 + \frac{\gamma}{2} \|\mathbf{d}_z^k - \mathbf{D}_z \mathbf{u} - \mathbf{b}_z^k\|_2^2. \end{aligned} \quad (11)$$

It is a convex function and equal to the following linear system

$$\begin{aligned} & (1 + \alpha \mathbf{D}_x^T \mathbf{D}_x + \beta \mathbf{D}_y^T \mathbf{D}_y + \gamma \mathbf{D}_z^T \mathbf{D}_z) \mathbf{u}^{k+1} \\ & = \mathbf{f} + \alpha \mathbf{D}_x^T (\mathbf{d}_x^k - \mathbf{b}_x^k) + \beta \mathbf{D}_y^T (\mathbf{d}_y^k - \mathbf{b}_y^k) \\ & + \gamma \mathbf{D}_z^T (\mathbf{d}_z^k - \mathbf{b}_z^k), \end{aligned} \quad (12)$$

which can be solved with a closed-form solution by the fast Fourier transform (FFT), (13) as shown at the bottom of this page, where $\mathcal{F}(\cdot)$ denotes the fast Fourier transform and $\mathcal{F}^{-1}(\cdot)$ the inverse transform. The superscript T is the operator of matrix transpose, and k is the iteration number.

- The \mathbf{d}_x -related subproblem is

$$\min_{\mathbf{d}_x} \lambda_1 \|\mathbf{d}_x\|_1 + \frac{\alpha}{2} \|\mathbf{d}_x - \mathbf{D}_x \mathbf{u} - \mathbf{b}_x\|_2^2. \quad (14)$$

$$\mathbf{u}^{k+1} = \mathcal{F}^{-1} \left(\frac{\mathcal{F} \left(f + \alpha \mathbf{D}_x^T (\mathbf{d}_x^k - \mathbf{b}_x^k) + \beta \mathbf{D}_y^T (\mathbf{d}_y^k + \mathbf{D}_y f - \mathbf{b}_y^k) + \gamma \mathbf{D}_z^T (\mathbf{d}_z^k - \mathbf{b}_z^k) \right)}{1 + \alpha (\mathcal{F}(\mathbf{D}_x))^2 + \beta (\mathcal{F}(\mathbf{D}_y))^2 + \gamma (\mathcal{F}(\mathbf{D}_z))^2} \right) \quad (13)$$

Algorithm 1 Image Destriping With ASSTV Algorithm

Input data \mathbf{f} , parameters $\lambda_1, \lambda_2, \lambda_3, \alpha, \beta$, and γ .

Initialize $\mathbf{u}_0 = \mathbf{f}, \mathbf{d}_x = 0, \mathbf{d}_y = 0, \mathbf{d}_z = 0$, and $\varepsilon = 10^{-3}$.

While ($\|\mathbf{u}^{k+1} - \mathbf{u}^k\| / \|\mathbf{u}^{k+1}\| > \varepsilon$ and $k < N_{\max}$) **do**

1. Update \mathbf{u}^{k+1} by (12)
2. Solve (17) for $\mathbf{d}_x^{k+1}, \mathbf{d}_y^{k+1}$, and \mathbf{d}_z^{k+1}
3. Update $\mathbf{b}_x^{k+1}, \mathbf{b}_y^{k+1}$, and \mathbf{b}_z^{k+1} by (18)

end While

Output: Destriping image = \mathbf{u}^{k+1}

It can be solved by using the soft shrinkage operator [37] as follows

$$\mathbf{d}_x^{k+1} = \text{shrink}(\mathbf{D}_x \mathbf{u}^{k+1} + \mathbf{b}_x^k, \frac{\lambda_1}{\alpha}), \quad (15)$$

where

$$\text{shrink}(r, \zeta) = \frac{r}{|r|} * \max(r - \zeta, 0). \quad (16)$$

This shrinkage operator requires only a few operations per element of \mathbf{d}_x . Similarly, \mathbf{d}_y^{k+1} and \mathbf{d}_z^{k+1} can be also derived simultaneously:

$$\begin{cases} \mathbf{d}_x^{k+1} = \text{shrink}(\mathbf{D}_x \mathbf{u}^{k+1} + \mathbf{b}_x^k, \frac{\lambda_1}{\alpha}) \\ \mathbf{d}_y^{k+1} = \text{shrink}(\mathbf{D}_y (\mathbf{u}^{k+1} - \mathbf{f}) + \mathbf{b}_y^k, \frac{\lambda_2}{\beta}) \\ \mathbf{d}_z^{k+1} = \text{shrink}(\mathbf{D}_z \mathbf{u}^{k+1} + \mathbf{b}_z^k, \frac{\lambda_3}{\gamma}). \end{cases} \quad (17)$$

Finally, the variables $\mathbf{b}_x^{k+1}, \mathbf{b}_y^{k+1}$, and \mathbf{b}_z^{k+1} are updated parallelly as follows:

$$\begin{cases} \mathbf{b}_x^{k+1} = \mathbf{b}_x^k + (\mathbf{D}_x \mathbf{u}^{k+1} - \mathbf{d}_x^{k+1}) \\ \mathbf{b}_y^{k+1} = \mathbf{b}_y^k + (\mathbf{D}_y (\mathbf{u}^{k+1} - \mathbf{f}) - \mathbf{d}_y^{k+1}) \\ \mathbf{b}_z^{k+1} = \mathbf{b}_z^k + (\mathbf{D}_z \mathbf{u}^{k+1} - \mathbf{d}_z^{k+1}). \end{cases} \quad (18)$$

In summary, the advantage of the split Bregman method is that the difficult optimization problem in (8) is split into the aforementioned four subproblems, which are relatively easy to optimize. The \mathbf{u} -related subproblem is accelerated by FFT efficiently, and $\mathbf{d}_x, \mathbf{d}_y, \mathbf{d}_z$ -related subproblems are solved by the efficient soft shrinkage operator with a computational complexity of $O(N^2)$. Moreover, $\mathbf{d}_x, \mathbf{d}_y$ and \mathbf{d}_z -related subproblems are independent and can be efficiently computed in parallel. Subsequently, $\mathbf{b}_x, \mathbf{b}_y$, and \mathbf{b}_z can be updated parallelly. This is the main reason why the split Bregman iteration works extremely fast on the proposed ASSTV image destriping model.

The algorithm procedure of ASSTV destriping method is summarized in **Algorithm 1**.

IV. EXPERIMENTS AND DISCUSSION

A. Experiment Setting

In the simulated experiments, part of the original hyperspectral cube of size $256 \times 256 \times 56$ was used to simulate the striped images by adding stripe lines to the original image. The data were provided by Professor David Landgrebe

and can be downloaded from [38], which were obtained via push-broom sensors. In real experiments, in order to verify the performance of the proposed algorithm for different types of stripes, we chose two types of satellite images: the cross-track-scanning-based MODIS images downloaded from [39] and the push-broom-scanning-based Hyperion images downloaded from [40]. The gray values of all the test images were normalized between [0, 1]. Note that, although we use the vector form to describe our method for clarity, in our implementation image cube data was computed still in 3D matrix format.

We compared the proposed algorithm with wavelet transform and adaptive frequency in [12] (WFAF), the total variation model in equation (4) (TV), the unidirectional TV algorithm in [21] (UTV), and the variational stationary noise remover algorithm in [25] (VSNR). The WFAF and VSNR algorithm implementations were kindly provided by Dr. Roshan Pande-Chhetri and Dr. Pierre Weiss, respectively.

Several qualitative and quantitative assessments were used to give an overall evaluation. The qualitative assessments included visual destriping inspection, the mean cross-track profile, and the power spectrum. The quantitative evaluation indices included peak signal-to-noise ratio (PSNR), structural similarity (SSIM) [41], Metric-Q [42], inverse coefficient of variation (ICV) [19], [21], noise reduction (NR) [19], [21], [26], and mean relative deviation (MRD) [19], [26]. The PSNR and SSIM are full-reference evaluation indices especially for the simulated experiments, whereas the others are no-reference evaluation indices. Metric-Q is used to assess the denoising performance, while ICV, NR and MRD are specific for evaluating the destriping performance. NR is the index to describe the ratio of stripes noise reduction in the frequency domain. ICV index evaluates the level of stripe noise and so would be calculated for homogeneous striped regions. On the contrary, MRD index is used to evaluate the performance of the algorithms to retain the information of image regions that are not affected by stripes, which measures the distortion caused by the destriping algorithms. In this paper, the definition of ICV, NR and MRD indices are directly referred to [19]. ICV index is computed in homogeneous regions within a window of 10×10 pixels, while MRD index is calculated in a 10×10 sharp region. The larger values of ICV and NR mean the better destriping performance. Conversely, the smaller MRD values denote the better destriping performance.

B. Simulated Experiments

In the simulated process, we added the synthetic stripe via observed model (1) on the base of the original hyperspectral image bands (band 31- band 40) in following five cases. From case 1 to case 4, we gradually increased the noise level by adding more striping lines. In case 5, we added stripes with a bigger variance than that in case 1, leading to a more severe striping effect. In all these cases, the locations of the stripes between the neighbor bands are different. We show the visual results of case 4 as an example, and the quantitative results of other cases are listed in Table I.

TABLE I
QUANTITATIVE EVALUATION RESULTS USING PSNR (dB) AND SSIM INDEXES OF HYPERSPECTRAL IMAGE BAND 37

Noise case	Index	Degraded	WFAF	TV	UTV	ASSTV
1	PSNR	30.28	38.73	31.86	39.02	46.89
	SSIM	0.8089	0.9763	0.8310	0.9794	0.9951
2	PSNR	27.27	41.62	30.98	42.74	43.78
	SSIM	0.6228	0.9797	0.7909	0.9872	0.9894
3	PSNR	22.49	39.38	28.58	41.55	42.28
	SSIM	0.4007	0.9676	0.6628	0.9838	0.9874
4	PSNR	17.28	32.64	22.69	33.16	36.57
	SSIM	0.1453	0.9326	0.4644	0.9343	0.9712
5	PSNR	20.73	30.32	26.14	30.52	32.09
	SSIM	0.4760	0.9027	0.5837	0.9197	0.9349

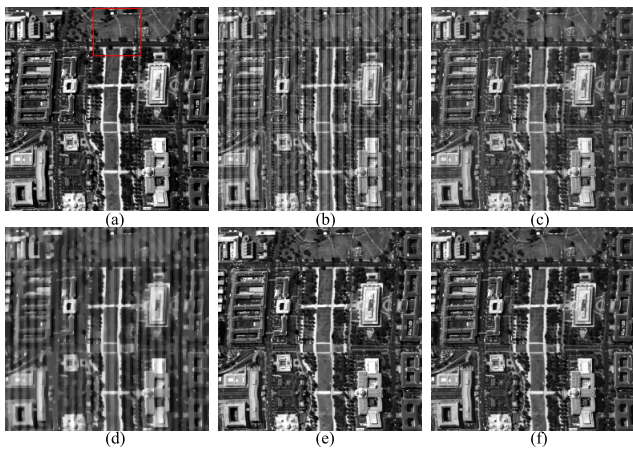


Fig. 5. Destriping results in simulated case 4. (a) Original hyperspectral image band 37. (b) Degraded with periodic stripes. Destriping results by (c) WFAF, (d) TV, (e) UTV, and (f) ASSTV.

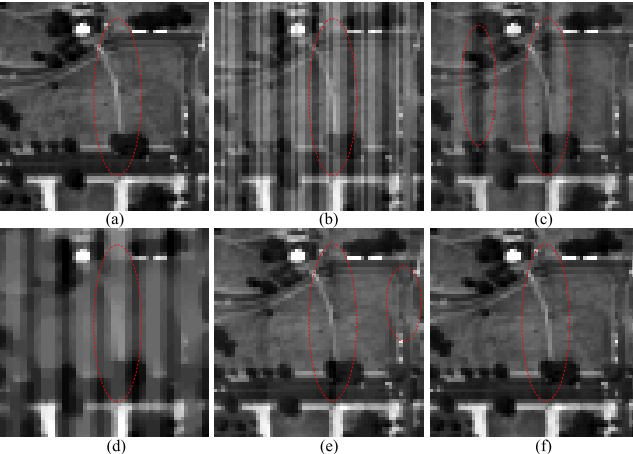


Fig. 6. Detailed regions cropped from Fig. 5. (a) Original image. (b) Degraded with periodic stripes. Destriping results by (c) WFAF, (d) TV, (e) UTV, and (f) ASSTV.

Figure 5(a) shows the original hyperspectral subimage of band 37. The striped image, shown in Fig. 5(b), is case 4. For convenience of comparison, the detailed regions cropped from Fig. 5 are displayed in Fig. 6. It is observed that the proposed ASSTV method obtains the best performance with respect to removing stripes, preserving details, and minimizing artifacts.

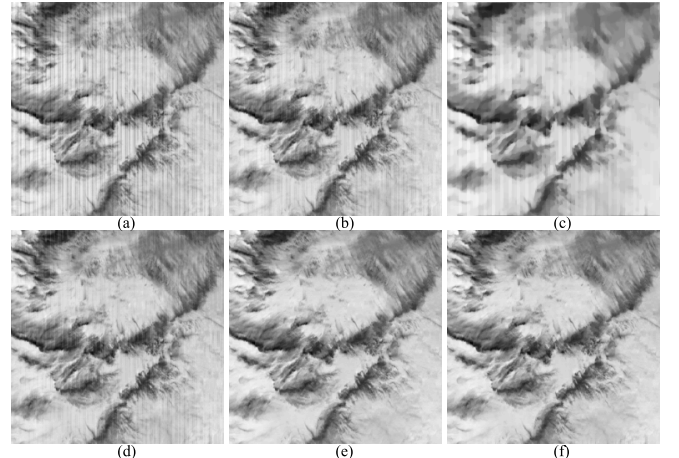


Fig. 7. Destriping results of regular periodic stripes. (a) Original MODIS image Terra band 28. Destriping results by (b) WFAF, (c) TV, (d) VSNR, (e) UTV, and (f) ASSTV.

In Fig. 6(c), although the stripes are well removed by WFAF method, some stripes-like artifacts, as indicated in the red ellipses, are unexpectedly introduced. This is because the edge structures with the same characteristic as the stripes are falsely regarded as the stripes and handled by WFAF method. Moreover, the contrast has been somehow decreased. The TV method has blurred the detail information, and the residual stripes still exist. Figure 6(e) shows the destriping result with UTV, wherein certain structures lying along the same direction as the stripes are degraded along with the stripes, as shown in the red ellipses. As mentioned above, the UTV approach lays emphasis on the smoothness of the images along a certain direction such that it tends to yield excessively destriped results. On one hand, the stripes are satisfactorily removed by ASSTV method; on the other hand, those structures lying along the same direction as the stripes are well preserved. Comparing Fig. 6(e) with Fig. 6(f), one can conclude that spectral consistency used in ASSTV model helps preserve the detail information substantially.

The quantitative assessments listed in Table I show that the ASSTV method gives the highest PSNR and SSIM values of all the methods. It is worth noting that the PSNR value of the degrade image in case 3 is 22.49 dB, while the proposed method improves the PSNR value by almost 20 dB in the presence of severe stripes.

C. Real Experiments

Figures 7-13 show the recovered results from all five methods on six real striped images, which differ from other types of stripes as shown in Fig. 1. The striped image selected from MODIS Terra band 28, as shown in Fig. 7(a), is highly contaminated by periodic stripes. Figure 8(a) shows periodic stripes with discontinuity, wherein the stripes do not run through the whole scan lines, as indicated by the elliptical mark. The burr-like stripes commonly exist at the dark regions in the MODIS images. Figure 9(a) is a subimage extracted from Hyperion image band 133. The stripes in MODIS image band 33, as shown in Fig. 11(a), appear as bright and dark

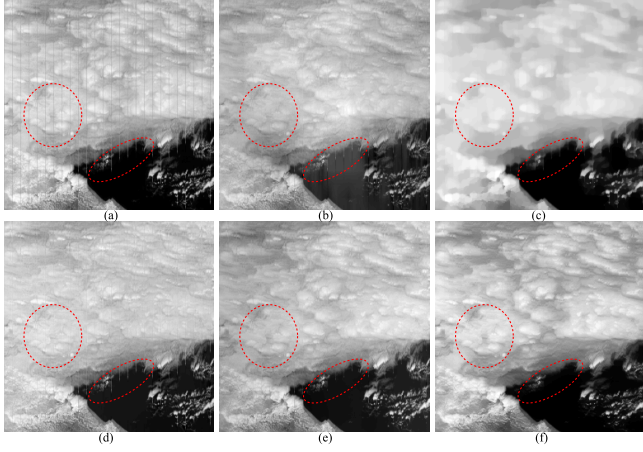


Fig. 8. Destriping results of periodic stripes with discontinuity. (a) Original MODIS image Aqua band 5. Destriping results by (b) WFAF, (c) TV, (d) VSNR, (e) UTV, and (f) ASSTV.

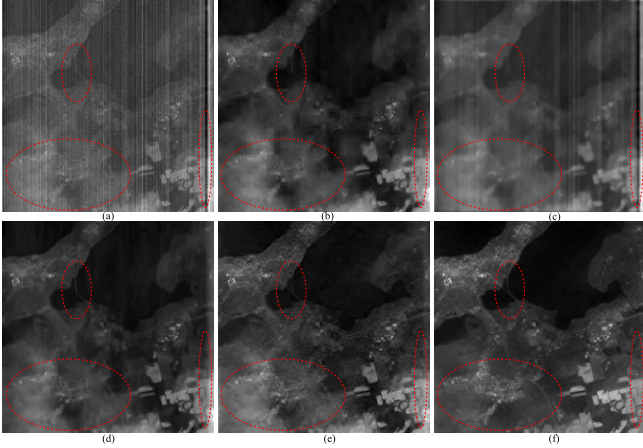


Fig. 9. Destriping results of non-periodic stripes with random width. (a) Original Hyperion image band 133. Restoration results by (b) WFAF, (c) TV, (d) VSNR+BM3D, (e) UTV+BM3D, and (f) ASSTV.

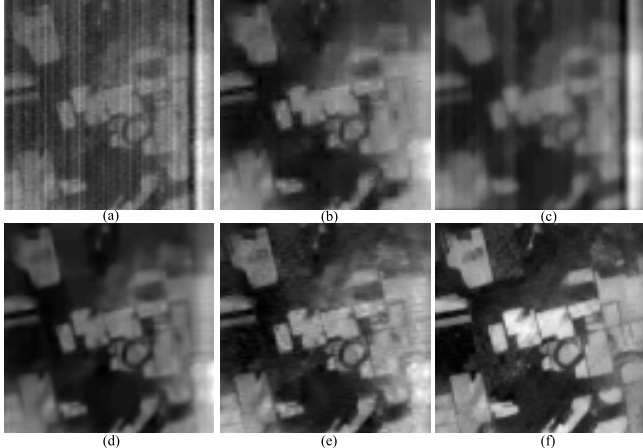


Fig. 10. Detailed regions cropped from Fig. 9. (a) Original image. Destriping results by (b) WFAF, (c) TV, (d) VSNR+BM3D, (e) UTV+BM3D, and (f) ASSTV.

lines with random lengths within a scan line. Figure 12(a) is a subimage extracted from MODIS image Aqua band 21, in which stripes and random noise coexist. In Fig. 13(a),

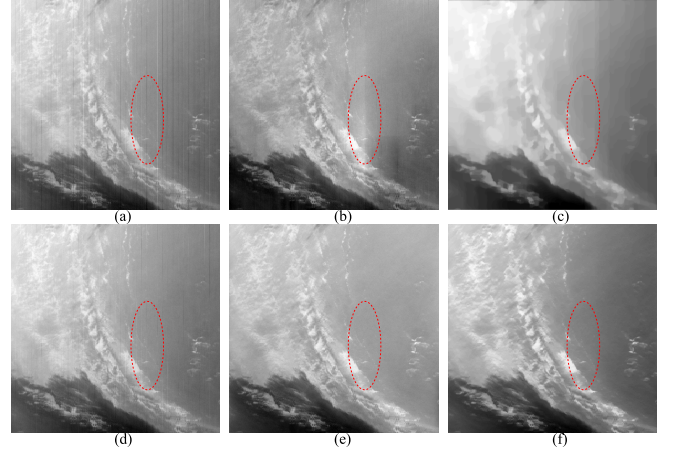


Fig. 11. Destriping results of non-periodic stripes with random length. (a) Original MODIS image band 33. Destriping results by (b) WFAF, (c) TV, (d) VSNR, (e) UTV, and (f) ASSTV.

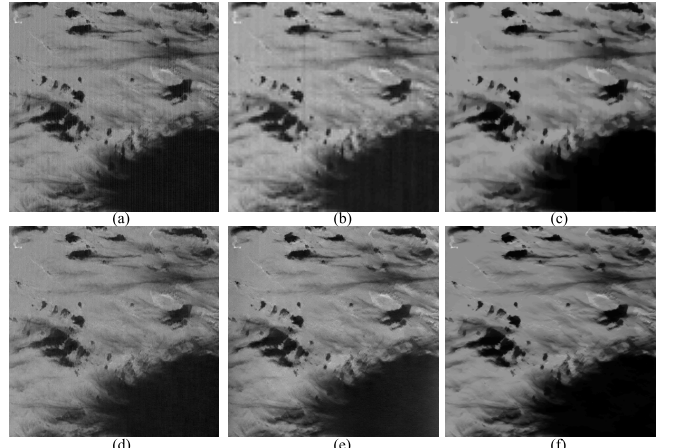


Fig. 12. Destriping results of moderate stripes and random noise. (a) Original MODIS image Aqua band 21. Destriping results by (b) WFAF, (c) TV, (d) VSNR, (e) UTV, and (f) ASSTV.

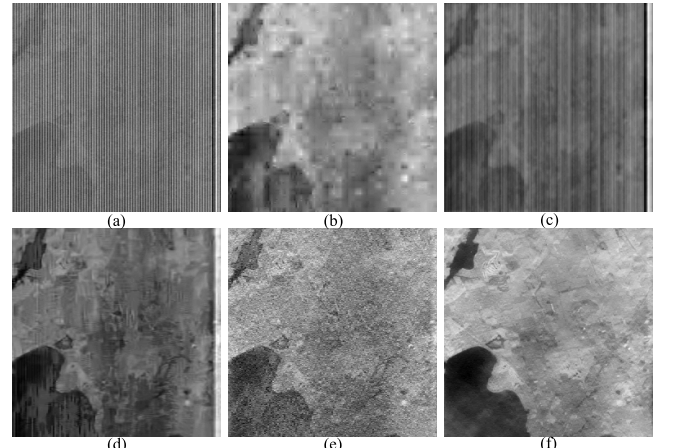


Fig. 13. Destriping results of severe stripes and random noise. (a) Original Hyperion image band 74. Destriping results by (b) WFAF, (c) TV, (d) VSNR, (e) UTV, and (f) ASSTV.

severe stripes and random noise overwhelm most of the useful information. It seems an impossible mission to recover from the single image.

TABLE II
QUANTITATIVE EVALUATION RESULTS USING METRIC-Q INDEX OF MODIS IMAGE AQUA BAND 21

Index	Original	WFAF	TV	VSNR	UTV	ASSTV
Metric-Q	9.31	13.21	18.72	5.29	9.38	16.85

TABLE III
QUANTITATIVE EVALUATION RESULTS USING ICV INDICES OF REAL IMAGES

Image	Area	Original	WFAF	TV	VSNR	UTV	ASSTV
Terra band28	Sample 1	15.73	41.40	40.87	55.03	105.13	135.63
	Sample 2	15.05	36.10	40.67	49.37	60.47	64.42
Aqua band5	Sample 1	17.97	19.64	25.52	20.43	18.45	19.82
	Sample 2	24.13	37.45	56.34	30.24	28.75	42.67
AVIRIS band133	Sample 1	6.24	6.60	12.97	7.46	6.09	9.55
	Sample 2	1.77	8.61	1.58	5.63	5.21	9.32
Terra band33	Sample 1	43.03	55.46	86.76	59.29	71.23	78.45
	Sample 2	17.89	25.40	41.55	33.21	50.45	54.70
Aqua band21	Sample 1	20.51	30.73	41.64	23.34	21.08	31.45
	Sample 2	25.84	68.48	181.75	28.48	32.61	63.76
AVIRIS band74	Sample 1	2.65	18.64	12.05	18.54	7.26	38.40
	Sample 2	2.59	13.74	10.80	11.63	8.21	28.01

It can be seen that ASSTV method significantly suppresses stripes with fewer artifacts, and consistently outperforms the compared methods with the best visual quality. Especially, for those stripes hard to be handled, residual stripes can be seen clearly in the results of other method. For example, the burr-like stripes still remain in the dark regions in Figs. 8(b)-8(e). Also, in the bottom-right red ellipse in Fig. 9(a), the stripes appear as bright or dark columns with considerable widths and useful information are totally overwhelmed by dead pixels. Since VSNR and UTV cannot handle the random noise in Fig. 9(a), we applied the BM3D denoising method [43] to their destriping results, as shown in Figs. 9(d) and 9(e). For convenience of comparison, the detailed regions cropped from Fig. 9 are displayed in Fig. 10. In Figs. 10(b)-10(e) by the compared methods, there more or less exist residual stripes, and blur effect is obvious. In contrast, in Fig. 10(f), the result image using the ASSTV method, not only the stripes and random noise are effectively removed, but also the detail structures are satisfactorily preserved.

Also, in Table II we list the quantitative index Metric-Q values to demonstrate the denoising performance in Fig. 12. It is shown that TV method obtains the highest Metric-Q value and ASSTV gets the second highest value. However, the TV method is at the cost of over smoothness, resulting in piecewise constant effects as shown in Fig. 12(c). On the contrary, the proposed ASSTV achieves a good balance between denoising and detail preservation in the destriping process.

Moreover, we compare the quantitative assessment ICV values of the tested methods in Table III. It can be seen that TV and ASSTV methods consistently obtain the best

ICV values, which means that the two methods always get the best destriping performance with little residual noise. However, these high ICV values of TV method are obtained at the expense of over smoothness and extremely poor visual quality in destriping results, which makes it inappropriate for real applications.

Table IV lists the NR and MRD values of MODIS images. As for NR index, we can find that ASSTV consistently obtain the best values, except for Aqua band 5. The main reason is TV method has over smoothed the result. As for MRD index, both VSNR and ASSTV have obtained quite satisfactory results. Overall, the quantitative results of the proposed method are consistent for all test images. Moreover, compared with other methods, ASSTV has obtained a satisfactory balance between stripe removal and information preserving.

Overall, the results of the proposed method are consistent for all test images, and exhibit good visual quality with fewer artifacts than the results obtained by the compared methods. Although the stripes are much related to the particular imaging platform, our general method captures two intrinsic characteristics of the striped remote sensing image cube: directional characteristic of stripes in spatial domain and spectral consistency characteristic in spectral domain. Every remote sensing striped image maintains these two characteristics, no matter where it comes from. That is the main reason why our ASSTV method works well on different stripe categories.

Moreover, there are two interesting phenomena on Hyperion images worth to be noticed. In Fig. 9(f), the proposed ASSTV method suppresses the light cloud in the bottom-left red ellipse, while other methods fail to achieve this. In Fig. 13(f), the ASSTV method removes severe stripes and random noise

TABLE IV
QUANTITATIVE EVALUATION RESULTS USING NR AND MRD INDICES OF MODIS IMAGES

Images	Index	WFAF	TV	VSNR	UTV	ASSTV
Terra band28	NR	6.69	6.06	10.42	12.45	12.90
	MRD	4.63%	5.34%	4.82%	4.92%	4.37%
Terra band33	NR	1.23	1.28	1.14	1.24	1.29
	MRD	10.03%	9.56%	2.82%	5.04%	3.14%
Aqua band5	NR	1.41	1.68	1.31	1.36	1.43
	MRD	14.53%	8.32%	3.41%	18.35%	1.67%
Aqua Band21	NR	1.06	1.24	1.26	1.18	1.31
	MRD	15.34%	5.95%	1.58%	8.69%	3.21%

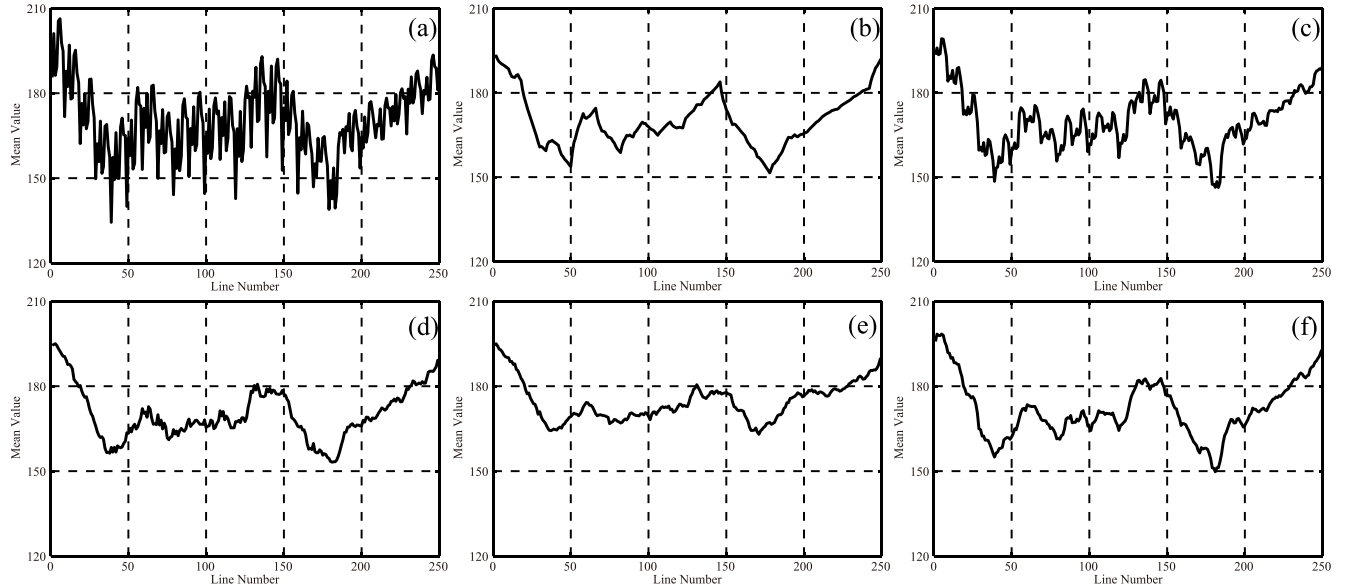


Fig. 14. The spatial mean cross-track profiles for images shown in Fig. 7. (a) Original image. Destriping results by (b) WFAF, (c) TV, (d) VSNR, (e) UTV, and (f) ASSTV.

simultaneously, and abundant structural information can be seen clearly. We attribute these interesting results to the spectral constraint along the spectral dimension in our model. Note that, the spectral consistency in Hyperion image is extremely high. Imposing a strong spectral smoothness constraint on the spectral direction, the neighbor bands will provide additional complementary information and help suppress the degradations in a certain band. But when spectral consistency is not guaranteed, it may introduce unnecessary artifacts across the bands. In this case, it needs to relax the spectral constrain (we will discuss it in the latter section). Therefore, it may well provide an alternative idea for cloud and random noise removal in multispectral or hyperspectral remote sensing image.

D. Discussion

1) *Spatial Analysis:* We test the performance of the proposed ASSTV method in spatial domain by two qualitative indices: mean cross-track profile and power spectrum. Figure 14 shows the spatial mean cross-track profiles of the MODIS image Terra band 28. The horizontal axis represents the column number, and the vertical axis represents the mean value of each column in certain band.

The mean cross-track profile of the striped image fluctuates wildly because of the stripes [Fig. 14(a)], while that of the healthy image exhibits a somewhat smoother curve.

In Figs. 14(c) and 14(d), we can observe some mild burrs in the curves, indicating that there are some residual stripes in their results. Figures 14(b), 14(e) and 14(f) all show satisfactory levels of smoothness. However, the images corresponding to Fig. 14(b) and 14(e) are over smoothed, and a considerable amount of detail information is lost. The reason for WFAF method is that the structure information has been corrupted in the filtering process, while the UTV model places too much constraint on the unidirectional derivative. The image corresponding to Fig. 14(f) achieves an acceptable tradeoff between stripe removal and detail preservation.

In Fig. 15, we plot the power spectrum of the MODIS image Terra band 28. For better visualization, the spectral magnitudes (the *y*-axis) are plotted with a logarithmic scale and the frequencies (the *x*-axis) are plotted with normalized frequency. In Fig. 15(a), there are several large impulses in the curve due to the effects of stripes. After destriping, although large impulses are greatly suppressed, there still exist light burrs, as

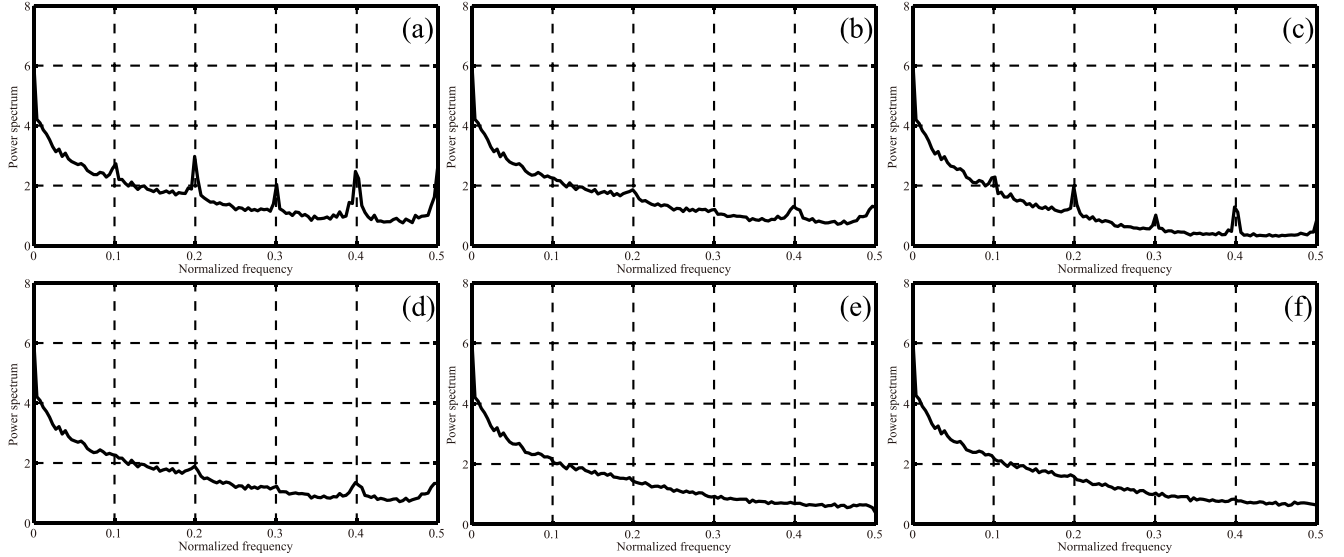


Fig. 15. The spatial power spectrums for images shown in Fig. 7. (a) Original image. Destriping results by (b) WFAF, (c) TV, (d) VSNR, (e) UTV, and (f) ASSTV.

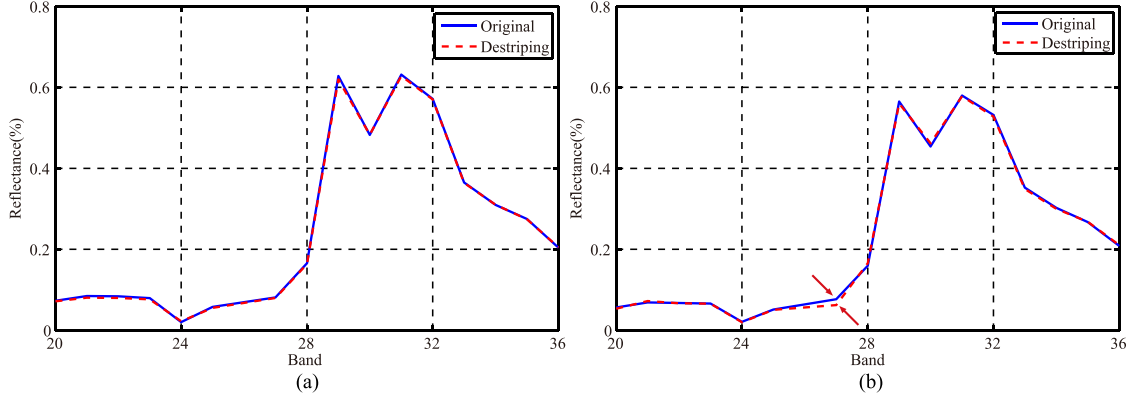


Fig. 16. Reflectance spectra for several pixels from MODIS Terra bands 20 to 36 before and after destriping. (a) Pixel 16384. (b) Pixel 10000.

shown in Figs. 15(b)-15(e); while in Fig. 15(f), the impulses are perfectly removed.

The main reason is that, the first and third terms of ASSTV model in Eq. (8) achieves reasonable information preserving ability, while the second and forth terms (Eq. (8)) can naturally produce a spatial-spectral smooth solution faithful to the input, vastly benefiting stripe removal. By balancing the regularization parameters, the ASSTV model can produce acceptable tradeoff between stripe removal and detail preservation with satisfactory results.

2) *Spectral Analysis:* Further, we attempt to demonstrate that ASSTV method can still preserve the useful spectral information while removing the noise from the spectral analysis. In Fig. 16, we show the reflectance spectra for pixels from the MODIS image Terra bands 20 to 36 (Corresponding to Fig. 7) before and after destriping. It can be seen in Fig. 16(a) that the spectral consistent information have been satisfactorily preserved. In Fig. 16(b), the stripe removal leads to a slight difference in reflectance value between before and after destriping in band 27.

3) *Regularization Parameters Selection:* In our model (8), there are three regularization parameters λ_1 , λ_2 , and λ_3 .

Parameter λ_1 and λ_2 depend on the stripe level, and larger values should be chosen for destriping severe stripes. Parameter λ_3 controls the contribution of the spectral smoothness according to spectral consistency. For image bands with low spectral consistency, one should select smaller λ_3 value in order to relax the spectral smoothness across the bands, or manually choose comparatively similar neighbor bands as input. To show their effects on the destriping performance, using simulated experiment case 4 as an example, we give a sensitivity analysis for the three parameters. Figures 17(a) - 17(c) show the change of the PSNR values with the change of the parameter λ_1 , λ_2 , and λ_3 , respectively. In Fig. 17(a), the highest PSNR value is achieved with parameter λ_1 between [0.1, 0.5]. From Fig. 17(b) and 17(c), it is shown that the destriping results exhibit robustness with the changes of parameter λ_2 and λ_3 . In all our implementations, we empirically set the parameter ranging as $\lambda_1 \in [0.01, 1]$, $\lambda_2 \in [1, 100]$, and $\lambda_3 \in [0.01, 10]$. The Bregman parameters were fixed as $\alpha = 10$, $\beta = 100$, and $\gamma = 10$.

Furthermore, we give the destriping results of Aqua band 1 to band 6 in Fig.18, and show heuristically how to set the regularization parameters. It is seen in the first row

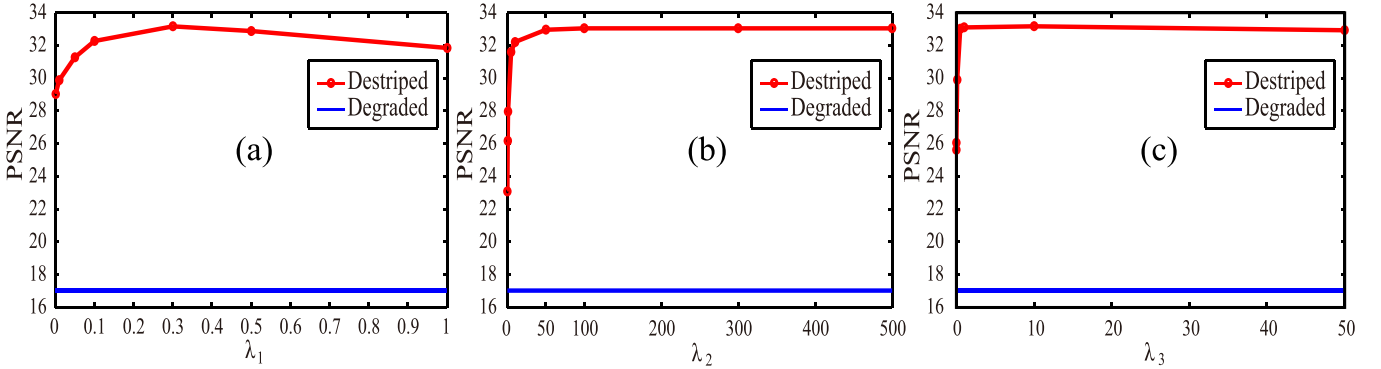


Fig. 17. Sensitivity analysis of regularization parameters λ_1 , λ_2 , and λ_3 . Change of the PSNR values versus the parameter (a) λ_1 , (b) λ_2 , and (c) λ_3 .

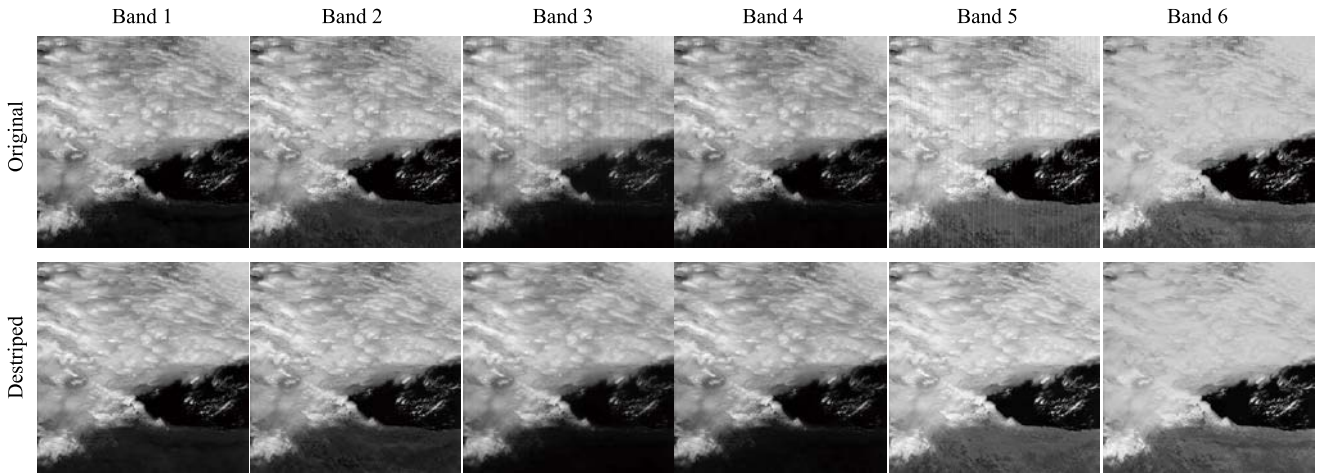


Fig. 18. Destriping results of MODIS Aqua cube with high spectral consistency.

that the original image of each band varies mildly, which means that the spectral consistency is relative high. Also, it can be observed that the mild stripes vary with different levels between bands. Thus, in this experiment, we set the parameter $\lambda_1=0.1$, $\lambda_2=1$, $\lambda_3=0.1$. In the second row, not only the stripes in all bands are removed satisfactorily, but also the structural information is well preserved.

4) *Number of Bands Selection*: For the proposed ASSTV method, the number of the bands is an important parameter. Note that, the number of the bands is highly related to the spectral consistency. In this section, we present an analysis about the effect of the band number on the destriping result. We choose simulated experiments case 1 (low noise level) and case 4 (high noise level) as the example. In Fig. 19, we show the changes of the PSNR and SSIM values with the different numbers of bands (from 2 to 11) under two noise levels.

From both Fig. 19(a) and 19(b), it can be seen that the destriping results become gradually better with larger number of bands. Nevertheless, when the number of bands is larger than 7, both PSNR and SSIM values increase a little but with extra computation and memory overheads. In our experiments, we empirically set the number of the bands as 10. Since hyperspectral image cube could offer dozens or even hundreds of bands, our ASSTV method can process the image cube group by group, with a group of 10 bands. ASSTV model works well when spectral consistency is guaranteed. How if this

condition is not provided? We performed another experiment to illustrate how to obtain good results for contiguous bands with far spectral distance.

Figure 20 shows the destriping results of MODIS image Terra from band 27 to 30 with far spectral difference. It can be seen that the original image of each band in the first row varies sharply, especially between band 28 and 29. The reason why we just heuristically choose four successive bands as illustration is that in low spectral consistency situation more input bands do not mean better destriping performance. In this experiment, we set the parameter $\lambda_1=0.5$, $\lambda_2=1$, $\lambda_3=0.01$. That is, in low spectral consistency situation with comparative small λ_3 and less image bands, ASSTV would be degenerated into spatial domain-based method and still work well. In the present work, we mainly consider the image bands with high spectral consistency. The adaptive method of selecting the number of bands and the spectral relationship are very interesting works, which are worth investigating in our future work.

5) *Running Time*: The proposed method obtains the clear image via (13), which is accelerated by FFTs. The three equations given by (17) can be computed via the shrinkage operate parallelly, which is extremely fast and requires only a few operations per element. Subsequently, the three equations given by (18) can be also calculated parallelly. All this ease of calculation makes the proposed method time-saving. We compare the running time of several representative

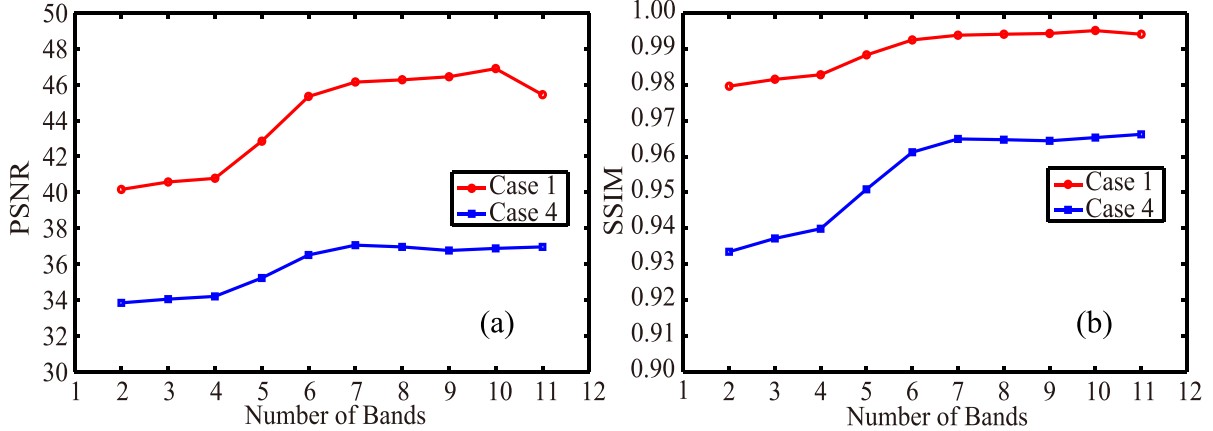


Fig. 19. Effects of the band numbers on destriping results under two noise levels. (a) PSNR and (b) SSIM values versus the band numbers.

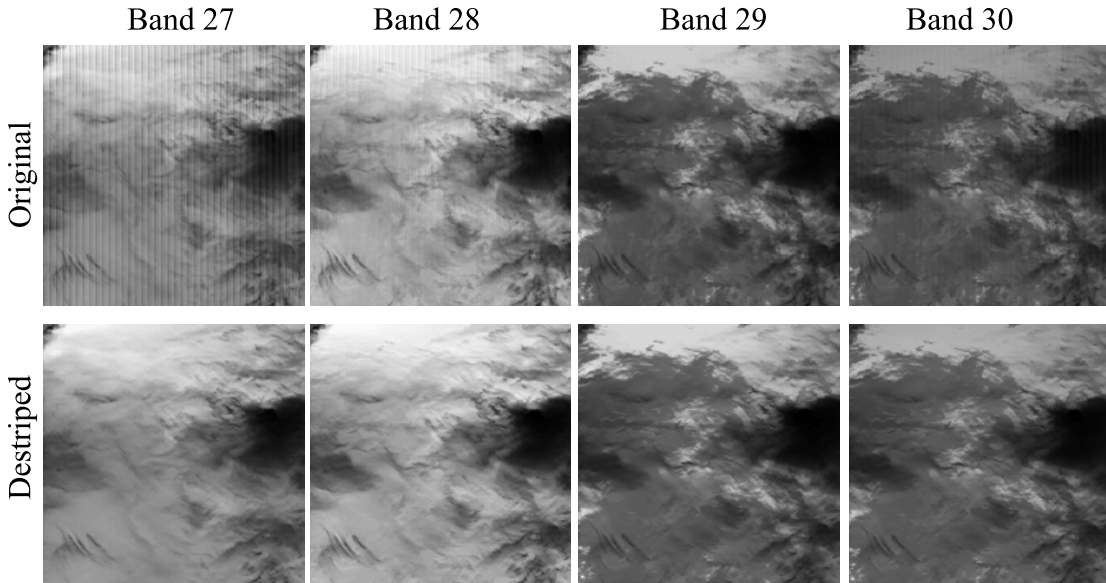


Fig. 20. Destriping results of MODIS Terra cube with low spectral consistency.

TABLE V
RUNNING TIME (IN SECONDS) OF DIFFERENT
METHODS IN THREE IMAGE SIZES

Size	WFAF	VSNR	UTV	ASSTV
256*256	0.28	4.05	6.25	0.35
400*400	0.37	23.32	46.75	0.90
1000*1000	1.23	159	498	5.95

destriping methods. Running time reported in Table V was obtained in Matlab 2010a on the same personal computer with an Intel i3 CPU at 3.4-GHz and 2-GB memory. It can be seen that the proposed method is quite fast, and can be further sped up in optimized C.

6) *Convergence*: We also test the convergence property of the proposed method. In this work, we use the normalized step difference energy (NSDE) defined as: $\|\mathbf{u}^{k+1} - \mathbf{u}^k\| / \|\mathbf{u}^k\|$ to illustrate the convergence rate. Figure 21 illustrates the evolutional curve of NSDE versus the iterations for MODIS image, whose result is shown in Fig. 7. It can be seen that the

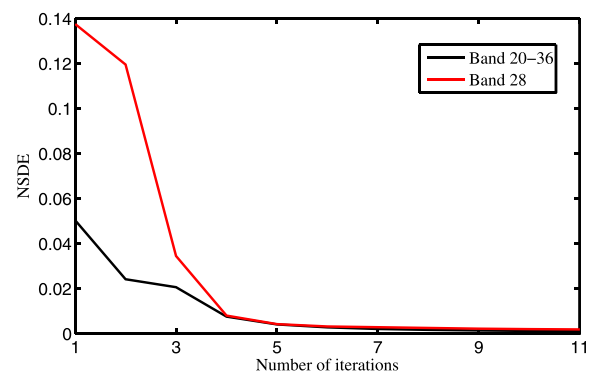


Fig. 21. NSDE versus the iteration number of the proposed method for Fig. 7.

proposed method achieves good convergence behavior in both the single band 28 and the whole volume, and converges after only 5 iterations.

7) *Limitations*: The proposed ASSTV method is effective for remove additive stripes. However, it can still be further improved in some aspects. In this paper, the parameters

are determined heuristically. Our future work will focus on automatically or adaptively selecting the parameters involved in the model. For instance, a monotonic decreasing weighted strategy related to the spectral distance between the adjacent bands can be integrated to adaptively adjust parameter λ_3 . For large spectral distance, parameter λ_3 will get a small value. Conversely, for small spectral distance, parameter λ_3 will get a large value.

V. CONCLUSION

The robustness for different stripes, preservation of detail information, and running time are difficult points and critical issues for image destriping algorithms. In this work, we firstly classify the stripe noise into a more comprehensive categorization. By analyzing the existing methods, we propose the anisotropic spectral-spatial total variation (ASSTV) regularization model, utilizing both the spectral consistent information in spectral domain and the directional information of stripes in spatial domain. Then, the fast optimization method, split Bregman iteration, is introduced to solve the resulting minimization problem. From the large set of experiments on both the qualitative and quantitative aspects, we have demonstrated the excellent effectiveness of the proposed method.

Although the denoising-based methods for image destriping are dominant, the image inpainting [44], [45] and image decomposition [46], [47] based methods are promising for the stripe removal. If we treat the stripes as the damages, such as scratches, the image inpainting methods can be naturally used. If we regard the striped image as the combination of clear image and stripe component, the image decomposition methods can be utilized. In future, we can incorporate these techniques into destriping.

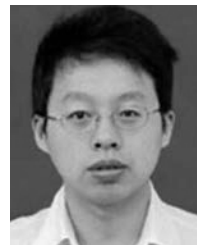
REFERENCES

- [1] M. Marconcini *et al.*, “Towards EO-based sustainable urban planning and management,” in *Proc. IEEE IGARSS*, Jul. 2013, pp. 4273–4276.
- [2] J. A. Richards and X. Jia, *Remote Sensing Image Analysis: An Introduction*, 4th ed. Berlin, Germany: Springer-Verlag, 1999.
- [3] Y. Chen, N. M. Nasrabadi, and T. D. Tran, “Hyperspectral image classification using dictionary-based sparse representation,” *IEEE Trans. Geosci. Remote Sens.*, vol. 49, no. 10, pp. 3973–3985, Oct. 2011.
- [4] M. Joshi and A. Jalobeanu, “MAP estimation for multiresolution fusion in remotely sensed images using an IGMRF prior model,” *IEEE Trans. Geosci. Remote Sens.*, vol. 48, no. 3, pp. 1245–1255, Mar. 2010.
- [5] P. Rakwatin, W. Takeuchi, and Y. Yasuoka, “Stripe noise reduction in MODIS data by combining histogram matching with facet filter,” *IEEE Trans. Geosci. Remote Sens.*, vol. 45, no. 6, pp. 1844–1856, Jun. 2007.
- [6] H.-S. Jung, J.-S. Won, M.-H. Kang, and Y.-W. Lee, “Detection and restoration of defective lines in the SPOT 4 SWIR band,” *IEEE Trans. Image Process.*, vol. 19, no. 8, pp. 2143–2156, Aug. 2010.
- [7] A. Barducci and I. Pippi, “Analysis and rejection of systematic disturbances in hyperspectral remotely sensed images of the Earth,” *Appl. Opt.*, vol. 40, no. 9, pp. 1464–1477, Mar. 2001.
- [8] L. Gómez-Chova, L. Alonso, L. Guanter, G. Camps-Valls, J. Calpe, and J. Moreno, “Correction of systematic spatial noise in push-broom hyperspectral sensors: Application to CHRIS/PROBA images,” *Appl. Opt.*, vol. 47, no. 28, pp. F47–F60, Oct. 2008.
- [9] Q. Yuan, L. Zhang, and H. Shen, “Hyperspectral image denoising employing a spectral-spatial adaptive total variation model,” *IEEE Trans. Geosci. Remote Sens.*, vol. 50, no. 10, pp. 3660–3677, Oct. 2012.
- [10] Y. Chang, L. Yan, H. Fang, and H. Liu, “Simultaneous destriping and denoising for remote sensing images with unidirectional total variation and sparse representation,” *IEEE Geosci. Remote Sens. Lett.*, vol. 11, no. 6, pp. 1051–1055, Jun. 2014.
- [11] J. Chen, Y. Shao, H. Guo, W. Wang, and B. Zhu, “Destriping CMODIS data by power filtering,” *IEEE Trans. Geosci. Remote Sens.*, vol. 41, no. 9, pp. 2119–2124, Sep. 2003.
- [12] R. Pande-Chhetri and A. Abd-Elrahman, “De-striping hyperspectral imagery using wavelet transform and adaptive frequency domain filtering,” *ISPRS J. Photogrammetry Remote Sens.*, vol. 66, no. 5, pp. 620–636, Apr. 2011.
- [13] B. Münch, P. Trtitk, F. Marone, and M. Stampanoni, “Stripe and ring artifact removal with combined wavelet–Fourier filtering,” *Opt. Exp.*, vol. 17, no. 10, pp. 8567–8591, May 2009.
- [14] F. Tsai and W. W. Chen, “Striping noise detection and correction of remote sensing images,” *IEEE Trans. Geosci. Remote Sens.*, vol. 46, no. 12, pp. 4122–4131, Dec. 2008.
- [15] F. L. Gadallah, F. Csillag, and E. J. M. Smith, “Destriping multisensor imagery with moment matching,” *Int. J. Remote Sens.*, vol. 21, no. 12, pp. 2505–2511, 2000.
- [16] B. K. P. Horn and R. J. Woodham, “Destriping LANDSAT MSS images by histogram modification,” *Comput. Graph. Image Process.*, vol. 10, no. 1, pp. 69–83, 1979.
- [17] M. Wegener, “Destriping multiple sensor imagery by improved histogram matching,” *Int. J. Remote Sens.*, vol. 11, no. 5, pp. 859–875, 1990.
- [18] G. Corsini, M. Diani, and T. Walzel, “Striping removal in MOS-B data,” *IEEE Trans. Geosci. Remote Sens.*, vol. 38, no. 3, pp. 1439–1446, May 2000.
- [19] H. Shen and L. Zhang, “A MAP-based algorithm for destriping and inpainting of remotely sensed images,” *IEEE Trans. Geosci. Remote Sens.*, vol. 47, no. 5, pp. 1492–1502, May 2009.
- [20] H. Carfantan and J. Idier, “Statistical linear destriping of satellite-based pushbroom-type images,” *IEEE Trans. Geosci. Remote Sens.*, vol. 48, no. 4, pp. 1860–1871, Apr. 2010.
- [21] M. Bouali and S. Ladjal, “Toward optimal destriping of MODIS data using a unidirectional variational model,” *IEEE Trans. Geosci. Remote Sens.*, vol. 49, no. 8, pp. 2924–2935, Aug. 2011.
- [22] J. Zhao *et al.*, “Single image stripe nonuniformity correction with gradient-constrained optimization model for infrared focal plane arrays,” *Opt. Commun.*, vol. 296, pp. 47–52, Jun. 2013.
- [23] Y. Chang, H. Fang, L. Yan, and H. Liu, “Robust destriping method with unidirectional total variation and framelet regularization,” *Opt. Exp.*, vol. 21, no. 20, pp. 23307–23323, Oct. 2013.
- [24] N. Acito, M. Diani, and G. Corsini, “Subspace-based striping noise reduction in hyperspectral images,” *IEEE Trans. Geosci. Remote Sens.*, vol. 49, no. 4, pp. 1325–1342, Apr. 2011.
- [25] J. Fehrenbach, P. Weiss, and C. Lorenzo, “Variational algorithms to remove stationary noise: Applications to microscopy imaging,” *IEEE Trans. Image Process.*, vol. 21, no. 10, pp. 4420–4430, Oct. 2012.
- [26] X. Lu, Y. Wang, and Y. Yuan, “Graph-regularized low-rank representation for destriping of hyperspectral images,” *IEEE Trans. Geosci. Remote Sens.*, vol. 51, no. 7, pp. 4009–4018, Jul. 2013.
- [27] H. Zhang, W. He, L. Zhang, H. Shen, and Q. Yuan, “Hyperspectral image restoration using low-rank matrix recovery,” *IEEE Trans. Geosci. Remote Sens.*, vol. 52, no. 8, pp. 4729–4743, Aug. 2014.
- [28] Y. Hu and M. Jacob, “Higher degree total variation (HDTV) regularization for image recovery,” *IEEE Trans. Image Process.*, vol. 21, no. 5, pp. 2559–2571, May 2012.
- [29] L. I. Rudin, S. Osher, and E. Fatemi, “Nonlinear total variation based noise removal algorithms,” *Phys. D, Nonlinear Phenomena*, vol. 60, nos. 1–4, pp. 259–268, 1992.
- [30] T. Chan, S. Esedoglu, F. Park, and A. Yip, “Recent developments in total variation image restoration,” in *Mathematical Models of Computer Vision*. New York, NY, USA: Springer-Verlag, 2005.
- [31] A. Lam, I. Sato, and Y. Sato, “Denoising hyperspectral images using spectral domain statistics,” in *Proc. Int. Conf. Pattern Recognit.*, Nov. 2012, pp. 477–480.
- [32] S. H. Chan, R. Khoshabeh, K. B. Gibson, P. E. Gill, and T. Q. Nguyen, “An augmented Lagrangian method for total variation video restoration,” *IEEE Trans. Image Process.*, vol. 20, no. 11, pp. 3097–3111, Nov. 2011.
- [33] E. Shechtman, Y. Caspi, and M. Irani, “Space-time super-resolution,” *IEEE Trans. Pattern Anal. Mach. Intell.*, vol. 27, no. 4, pp. 531–545, Apr. 2005.
- [34] B. Rasti, J. R. Sveinsson, M. O. Ulfarsson, and J. A. Benediktsson, “Hyperspectral image denoising using 3D wavelets,” in *Proc. IEEE Int. Geosci. Remote Sens. Symp. (IGARSS)*, Jul. 2012, pp. 1349–1352.

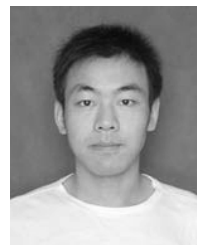
- [35] Y. Qian and M. Ye, "Hyperspectral imagery restoration using nonlocal spectral-spatial structured sparse representation with noise estimation," *IEEE J. Sel. Topics Appl. Earth Observ.*, vol. 6, no. 2, pp. 499–515, Apr. 2013.
- [36] T. Goldstein and S. Osher, "The split Bregman method for L1-regularized problems," *SIAM J. Imag. Sci.*, vol. 2, no. 2, pp. 323–343, May 2009.
- [37] D. L. Donoho, "De-noising by soft-thresholding," *IEEE Trans. Inf. Theory*, vol. 41, no. 3, pp. 613–627, May 1995.
- [38] *Hyperspectral Images*. [Online]. Available: <https://engineering.purdue.edu/~biehl/MultiSpec/hyperspectral.html>, accessed Sep. 2013.
- [39] *MODIS Level 1, Atmosphere and Land Data Products*. [Online]. Available: <http://ladsweb.nascom.nasa.gov/>, accessed May 2013.
- [40] *Hyperion Hyperspectral Image Data*. [Online]. Available: <http://compression.jpl.nasa.gov/hyperspectral/imagedata/>, accessed May 2013.
- [41] Z. Wang, A. C. Bovik, H. R. Sheikh, and E. P. Simoncelli, "Image quality assessment: From error visibility to structural similarity," *IEEE Trans. Image Process.*, vol. 13, no. 4, pp. 600–612, Apr. 2004.
- [42] X. Zhu and P. Milanfar, "Automatic parameter selection for denoising algorithms using a no-reference measure of image content," *IEEE Trans. Image Process.*, vol. 19, no. 12, pp. 3116–3132, Dec. 2010.
- [43] K. Dabov, A. Foi, V. Katkovnik, and K. Egiazarian, "Image denoising by sparse 3D transform-domain collaborative filtering," *IEEE Trans. Image Process.*, vol. 16, no. 8, pp. 2080–2095, Aug. 2007.
- [44] R. H. Chan, J. Yang, and X. Yuan, "Alternating direction method for image inpainting in wavelet domains," *SIAM J. Imag. Sci.*, vol. 4, no. 3, pp. 807–826, 2011.
- [45] M. Bertalmio, G. Sapiro, V. Caselles, and C. Ballester, "Image inpainting," in *Proc. 27th SIGGRAPH*, 2000, pp. 417–424.
- [46] J.-L. Starck, M. Elad, and D. L. Donoho, "Image decomposition via the combination of sparse representations and a variational approach," *IEEE Trans. Image Process.*, vol. 14, no. 10, pp. 1570–1582, Oct. 2005.
- [47] S. Osher, A. Sole, and L. Vese, "Image decomposition and restoration using total variation minimization and the H^1 norm," *Multiscale Model. Simul.*, vol. 1, no. 3, pp. 349–370, 2003.



Yi Chang received the B.S. degree in automation from the University of Electronic Science and Technology of China, Chengdu, China, in 2011, and the M.S. degree in pattern recognition and intelligent systems from the Huazhong University of Science and Technology, in 2014. His current research interests include image processing and distance metric learning.



Luxin Yan (M'12) received the B.S. degree in electronic communication engineering and Ph.D. degree from the Huazhong University of Science and Technology (HUST), in 2001 and 2007, respectively. He is currently an Associate Professor with the Institute for Pattern Recognition and Artificial Intelligence, HUST. His current research interests include multispectral image processing and pattern recognition.



Houzhang Fang (S'12) received the M.S. and Ph.D. degrees in applied mathematics and control science from the Huazhong University of Science and Technology, in 2010 and 2014, respectively. He is currently a Lecturer with Xidian University. His research interests include image restoration, blind image deconvolution, object detection, and recognition.



Chunan Luo received the B.S. degree in electrical engineering and automation from Central South University, Changsha, China, in 2013. He is currently pursuing the M.S. degree with the Institute for Pattern Recognition and Artificial Intelligence, Huazhong University of Science and Technology, Wuhan, China. His research interests include image processing and machine learning.